

# Viscous Effects on the Instability of an Axisymmetric Jet

K.B.M.Q. Zaman  
*Lewis Research Center*  
*Cleveland, Ohio*

and

J.M. Seiner  
*Langley Research Center*  
*Hampton, Virginia*

February 1990



(NASA-TM-102396) VISCIOUS EFFECTS ON THE  
INSTABILITY OF AN AXISYMMETRIC JET (NASA)  
28 p CSCL 01A

N90-16719

Unclass

G3/02 0264827

# VISCOUS EFFECTS ON THE INSTABILITY OF AN AXISYMMETRIC JET

K.B.M.Q. Zaman  
National Aeronautics and Space Administration  
Lewis Research Center  
Cleveland, Ohio 44135

and

J.M. Seiner  
National Aeronautics and Space Administration  
Langley Research Center  
Hampton, Virginia 23665

## ABSTRACT

The stability characteristics of a laminar, axisymmetric jet, issuing from fully developed Poiseuille flow, are investigated. The jet preferred frequency, as inferred from surveys of  $u'$ -spectra, is found to yield a Strouhal number ( $St$ ) that depends on the Reynolds number ( $R$ );  $St$  and  $R$  are based on the jet diameter ( $D$ ) and the average velocity ( $U_{av}$ ) at the jet origin. The value of  $St$  increases with increasing  $R$  in the range  $400 \leq R \leq 4000$ , attaining an asymptotic value of about 0.45. Flow visualization confirms that the instability is primarily in a helical mode, as predicted by stability analyses. Analyses do predict a similar  $St$  versus  $R$  variation in approximately the correct  $St$ -range. However, the  $R$ -range where this is predicted is lower than that found experimentally.

## 1. INTRODUCTION

The instability and transition of low Reynolds number jets have been the subject of many previous experimental investigations. Addressed among other questions were, the critical Reynolds number,<sup>1,2</sup> the distance of the transition point from the jet origin,<sup>3</sup> and the nature of the instability process leading to turbulence.<sup>2,4-6</sup> Several investigated the preferred frequency of sensitivity ( $f_m$ ) of these jets either through observation of the naturally growing instability waves or through external perturbation techniques.

However, a variety of scaling laws for  $f_m$ , some conflicting with one another, were reported for jets with various nozzle geometries. These are summarized in Table 1.

The scaling,  $St \propto R^{0.5}$ , in the initial region of a top-hat jet with thin boundary layer, is relatively well understood. The frequency  $f_m$  for the efflux shear layer scales as the characteristic layer thickness which in turn varies as  $R^{-0.5}$ , yielding the above proportionality.<sup>12</sup> In contrast, in a top-hat jet with thick boundary layer, preliminary results of this study as well as Anderson's,<sup>10</sup> exhibited the tendency towards a constant Strouhal number. On the other hand, for  $R \lesssim 3000$ , the  $St$  versus  $R$  scaling obviously varied widely with nozzle geometry.

Some of the differences in the data in Table 1 are likely to be due to differences in the initial mean velocity profiles, which were not measured in these older studies. Unfried's<sup>11</sup> jet, presumably with initially parabolic profile, seemed comparable to the present jets. The  $R$ -dependence of  $St$  observed by Unfried agreed in general trend with our preliminary data in the tube geometry as well as with Rockwell's<sup>13</sup> in low Reynolds number slit jets. However, it was far from clear from physical reasonings why a particular power-law for the  $St$  versus  $R$  variation should occur. On the other hand, one would expect that such a trend be predicted by stability analysis when viscous effects were included; but this was not readily apparent in the published stability analysis results.

These provided the motivation for carrying out a controlled experiment. An added motivation stemmed from the idea that such a jet would assume a bell-shaped mean velocity profile while staying laminar, and thus, provide a conducive environment for investigation of the corresponding stability characteristics. The relevance of the bell-shaped profile is that it characterizes the asymptotic region of all axisymmetric jets.

The experiments were started in a jet issuing from a 2.54 cm diameter, 4.27 m long pipe. However, even though the flow in this case stayed laminar at much higher  $R$ , a developed parabolic velocity profile occurred only for very low  $R$  (discussed further in the text). At the low  $R$  the corresponding jet velocities were low and were affected by residual room drafts. Thus, it was necessary to revert to smaller diameter tubes in order to carry out meaningful hot-wire measurements. During these preliminary investigations it was observed that the velocity spectrum, measured within the laminar lengths of these jets, was consistently characterized by a broadband but unambiguous hump. The center frequency of this hump, whose significance is addressed in the text, has been considered the preferred frequency  $f_m$  of the jet. A parametric study of  $f_m$ , while ensuring parabolic initial mean velocity profile, was the specific objective in the experiment. The corresponding  $St$  versus  $R$  relationship was then examined, and an attempt made to explain the result in the light of stability analysis.

## 2. EXPERIMENTAL FACILITIES

The jets were formed by passing compressed air through a stainless steel tube; a schematic of the flow facility is shown in Fig. 1(a). The tube had an internal diameter of 2.3 mm and a length to diameter ratio ( $L/D$ ) of about 600. It was mounted on an optical bench and adjusted so that the axis of the issuing jet was within  $0.5^\circ$  of the streamwise probe traversing axis. The jet axis was determined by appropriate velocity profile measurements. An automated traversing mechanism enabled accurate hot-wire probe positioning in the cross stream plane. The streamwise distance ( $x$ ) from the tube exit was set within a resolution of  $\pm 0.5$  mm by sliding the mechanism on the optical bench.

The entire set-up was installed in a 2.4 by 3 by 3.7 m anechoic chamber. All data acquisition were done remotely from outside the chamber. The volume flow rate was measured by a laminar flow element (Merian 50MJ10). The

measured flow rate checked out well with corresponding estimates from the exit velocity profiles measured by the hot-wire. Velocity spectra measurements were done by a SD380 FFT analyzer. Data acquisition and analysis were done by a (Microvax II) minicomputer.

In order to address the effect of probe resolution in the present measurements (see section 3.2), four different hot-wire probes having different sizes relative to the jet were used. Characteristics of the probes are listed in Table 2. Note that probe 1 has a large overall wire length, so that it spanned the entire jet. This way, the prongs were out of the flow and thus the flow disturbances were minimal. Probes 2 and 4 were specially fabricated, while probe 3 was another commercially available one. The latter three are shown by the photographs in Fig. 1(b) with the tube exit as background. Probe 1, not shown in Fig. 1(b), would appear similar to probe 4 having its prongs out of the field of view. Its active wire length, situated in the middle, is comparable to that of probe 3. The probes were calibrated in a small wind tunnel.

Most data reported were obtained with probes 1 and 2. Probe 1 was used in the original experiment, during the period 1983-84. The experiment was repeated later with probes 2 to 4, in 1987. At the later time some of the instrumentation was different from but functionally the same as discussed above. All air jet experiments were done in the anechoic chamber at the NASA Langley Research Center.

The flow visualization experiment was carried out with a 1.1 mm diameter water-in-water jet at the NASA Lewis Research Center, in 1987. The corresponding details are discussed together with the results in the following text.

### 3. RESULTS AND DISCUSSION

#### 3.1 Velocity Profiles

Radial profiles of the longitudinal mean velocity ( $U$ ) are shown in Fig. 2(a) for three Reynolds numbers,  $R = U_{av}D/\nu$ . Parabolic profiles have been fitted to the data to match the measured peak velocity, and are shown by the solid lines. It is clear that fully developed parabolic  $U$ -profile existed even at the highest  $R$ ; above about  $R = 4000$  the flow became turbulent. It is worth mentioning that in a larger tube ( $D = 1$  cm;  $L/D = 600$ ), laminar flow could be maintained at much higher  $R$  ( $\approx 10^4$ ), but for  $R \geq 5000$ , the profiles tended to become skewed, i.e., the maximum occurred off-center, the reason for which remains unknown. As mentioned before, in an even larger tube ( $D = 2.54$  cm,  $L/D = 168$ ), laminar flow could be maintained up to  $R \approx 3 \times 10^4$ , but the profiles were not fully developed.

The jets stayed laminar for considerable distance ( $x$ ) from the tube exit, the laminar length decreasing with increasing  $R$ . Radial  $U$ -profiles at  $x/D = 15, 20$  and  $30$  for  $R = 2000$ , within the laminar length, are shown in Fig. 2(b). It appears that by the distance  $x/D = 15$  the  $U$ -profile has attained a bell shape. The measured jet diameter ( $D_{0.5}$ ), spanning the points where the velocity was half the local maximum, increased only slightly within the axial distance covered in Fig. 2(b). This increase is within 4 percent of an average value of  $D_{0.5}$ . The centerline mean velocity ( $U_c$ ), however, has decreased by about 30 percent of the corresponding average value of  $U_c$ . The large difference between the rates of changes of  $D_{0.5}$  and  $U_c$  indicates that the profiles are still evolving and have not attained self-similarity. In the  $x$ -range covered, the spread rate,  $\delta D_{0.5}/\delta x$ , is about 0.002; the rate,  $(D/2U_{av})(\delta U_c/\delta x)$ , is about -0.015. These rates, due primarily to viscous diffusion, are small compared to the rates 0.172 and -0.194, respectively, found for the asymptotic region of a turbulent jet.<sup>14</sup>

### 3.2 Probe Resolution

Because of the finite size of the hot-wire probe relative to the jet, there is spatial averaging in the data of Fig. 2. The probe length ( $\ell$ ) was approximately one quarter of the jet diameter ( $D$ ). However, the averaging is not severe as the following estimates should show. With the probe placed on the jet axis, assuming uniform temperature distribution over  $\ell$ , the measured velocity can be estimated to be  $u_{\text{meas}} = u_{\text{actual}}[1 - (1/3)(\ell/D)^2]$ , where  $u_{\text{actual}}$  is the corresponding true velocity. Thus, with probe 2 the centerline velocity is underestimated by about 2.6 percent. The averaging is progressively larger on the edges of the jet. The error can be shown in a similar manner to be still less than 10 percent up to a point where the local velocity is 30 percent of the centerline velocity. Furthermore, the effect of end conduction in the probe is to reduce the effective length,<sup>15</sup> and thus the errors should be actually even smaller than the above estimates.

Let us consider the effect of finite probe length on the measurement of  $u'$ -spectra. As hot-wire signals represent a line average of fluid activity, the sensing length in general must be small compared to the smallest wavelength to be measured.<sup>16</sup> The sensor dimension must be less than one half the size of the smallest scales to avoid aliasing. Furthermore, the length to diameter ratio of the sensor must also be large (about 200 or larger) in order to avoid distortion of spectral shape arising from end conduction effects.<sup>15,16</sup> The latter constraint puts a limit to the minimum permissible length for a sensor of given diameter. In consideration of these, the sensors that could be developed, allowing reliable continued operation, still turned to be large. The smallest was approximately one quarter the diameter of the jet (Table 2).

However, in spite of the finite probe size the measured  $u'$ -spectra are free of significant aliasing effect. This is demonstrated by the spectra in Fig. 3, measured with probes 2 to 4 at the same location (on the axis at

$x/D = 20$ ). First, it is observed that the spectral shapes are identical for probes 2 and 3 in spite of a 2:1 ratio of the sensor lengths. These two traces, although staggered in Fig. 3 for clear identification, would match almost exactly if overlayed. If there was aliasing, these would be different and probe 3 spectrum should have exhibited higher energy content on the low frequency end.

The negligible aliasing in the spectra follows from the fact that the wavenumber vectors associated with the instability waves, within the laminar lengths, are primarily aligned with the streamwise direction. Thus, the measurement concerns a one-dimensional wavenumber space in which the pertinent sensor dimension is the sensor diameter and not the length. An analogy can be made with the situation where a finite length single hot-wire is used to make measurements in a thin boundary layer, by orienting the wire such that the wire diameter determines the spatial resolution. Thus, as far as the spectral shapes are concerned, any of probes 2 and 3 seemed adequate. A mean frequency corresponding to the peak in each of the spectra from the two probes is read to be the same (about 2.05 kHz).

With probe 4, only a third of the active length was exposed to the jet. The hot-wire response in this case is complicated due to the grossly nonuniform temperature distribution along the wire length. Conduction effects along the wire should be significant compared to the convective heat transfer. Freymuth<sup>17</sup> discussed the effect of end conduction on the frequency response of hot-wires. He quoted previous experiments showing that the hot-wire output was attenuated at higher frequencies when conduction effects were significant. Thus, a shift of a broadband spectral peak to lower frequencies may be expected qualitatively with probe 4. A mean frequency read from probe 4 spectrum in Fig. 3 is indeed slightly less than that read from the other two spectra. Nevertheless, the discrepancy for the case documented is very small, the



spectral shape obtained with probe 4 being quite similar to the other two. However, use of probe 4 was avoided in the subsequent measurements.

Any of probes 1 to 3 having a sensor length smaller than the jet diameter was considered adequate for the following measurements. Probe 1 had the advantage of having its prongs out of the flow. Data taken with both probes 1 and 2 are presented, the probe in use being identified in the figure caption.

### 3.3 Spectral Evolution

The onset of instability and transition with increasing  $x/D$  are illustrated in Fig. 4 by the velocity spectra measured on the jet axis. Note that the spikes in the spectra are due to 60 Hz line hum and its harmonics. The total root mean square velocity fluctuation within the laminar lengths were small and within 2 percent of  $U_{av}$ . Thus, the electronic noise showed up prominently in the spectra. The 60 Hz spikes were less prominent when the linearizer was taken out of the anemometer circuitry. However, for measurement convenience the linearizer was used. Let us also mention that except for the 60 Hz spikes, the spectrum at the jet exit was completely free of any peaks.

With increasing  $x$ , a distinct spectral hump appears after a certain location ( $x_I$ ). The trace at the bottom of Fig. 4 corresponds to this location. The hump grows in amplitude until, at a farther location  $x_T$  ( $\approx 30D$ ), a sudden increase in the broadband components commences. Here the total root mean square intensity exceeded 20 percent of  $U_{av}$ . The latter location is also characterized by a sudden drop in the mean velocity as measured on the axis.  $x_I$  and  $x_T$  measured for a few  $R$  are listed in Table 3. These data are further discussed in section 3.4.

The significance of the spectral humps (Fig. 4) should be considered. The humps are due to the energetic instability waves in the jet. If the instability was periodic, the spectrum would be marked by a sharp spike at the corresponding frequency. In a natural flow, there are departures from strict

periodicity resulting in a broadband peak or hump. Such broadband spectral peaks characterize various other shear flows, e.g., cold top-hat jets,<sup>18</sup> single stream mixing layers.<sup>19</sup> From a physical point of view, the spectral humps merely represent the energy content in the dominant instability waves, a mean frequency within the band corresponding to the most energetic of the waves. An area-averaged mean frequency of the spectral hump is referred to in the following as the preferred frequency,  $f_m$ .

The nature of the velocity fluctuations represented by the spectral humps in Fig. 4 should also be considered. Theoretical as well as experimental evidence almost exclusively suggest that jets with parabolic or bell-shaped U-profiles are unstable only to disturbances of the helical type; the  $n = 1$  mode being dominant. (See, Refs. 20 to 23 for analysis, and Refs. 4, 6 and the visualization pictures in the following for experimental evidence.) The streamwise velocity fluctuation due to a helical instability is zero on the jet axis. However, the spectra in Fig. 4, which represent measurements on the jet axis, also contain transverse velocity fluctuation based on normal wall cooling, and off-axis streamwise fluctuation due to the finite sensitive wire length. Thus, although one cannot infer from the present hot-wire measurements the exact nature of the instability waves, the frequencies should be well represented. In fact, the measured spectral shapes are found to be invariant of the radial locations in the jet.

Velocity spectra measured at different radial locations, at  $x/D = 20$  for  $R = 2000$ , are shown in Fig. 5. These data were taken with probe 2 whose prongs entered the flow while making measurements especially on the negative radii locations (traces f to i). As a result, the flow disturbances contaminated the spectral shapes on that side which is clear for the 30 percent velocity point case. Measurements with probe 1, at corresponding locations on either side of the jet axis (not shown), produced identical pairs of spectra. Thus, the

spectral shapes, and  $f_m$ , are found to remain essentially unchanged across the jet.

Before examining the parametric dependence of  $f_m$  let us consider the nature of the instability waves from the flow visualization experiment.

### 3.4 Flow Visualization

The visualization experiments were carried out in a small water tunnel, having 7.6 cm high by 30.5 cm wide by 48.3 cm long test section. A 1.1 mm i.d. stainless steel tube, having  $L/D = 600$ , was mounted horizontally with the tube exit positioned near the middle of the test section entrance. Water mixed with a small amount of fluorescent dye, kept in a large reservoir, was forced through the tube by pressurized air. The jet issued into the still water that filled the test section. The flow rate was measured simply by timed collection of the water into a reservoir, in the empty test section, and was calibrated against the driving air pressure. Large pressures were required, e.g., about 5 psig to obtain  $R = 1000$ ; thus, error due to change in the differential pressure when the test section was filled with water was ignored. The issuing jet was viewed with flood light and photographed using a 35 mm camera.

A sequence of photographs for varying  $R$  is shown in Fig. 6. In each, the jet origin is on the left and the field of view covers approximately  $130^\circ$ . At lower  $R$  ( $<400$ ), the jet stayed laminar throughout the test section into the downstream reservoir; this distance covered at least  $400D$ . Note that at the lowest  $R$  ( $\approx 150$ ) the viscous diffusion and the consequent spread rate of the jet are visibly higher. This is consistent with predictions for a laminar jet. Following Schlichting's<sup>24</sup> solution, one can show that the jet half-velocity-diameter ( $D_{0.5}$ ) should vary as,  $D_{0.5}/D = (10.3/R)(x/D)$ . Thus, the jet spread rate should be more at lower  $R$ .

Transition to turbulence is seen to occur within the viewing length when the Reynolds number is about 400. The long laminar lengths at low  $R$  was a

subject of controversy which was addressed by Reynolds.<sup>2</sup> The analytically predicted critical  $R$  is much lower, e.g., about 33 in Kambe's<sup>21</sup> analysis. Such a prediction was well supported by the experimental result of Viilu<sup>1</sup> who found the stable-unstable transition at about  $R = 11$ . However, Viilu's observation conflicted with an earlier experiment by H. Schade<sup>2</sup> in which, as in the present experiment, rectilinear laminar jets were observed at  $R$  values of several hundreds. Reynolds' subsequent experiment revealed that transition did occur at very low  $R$ , agreeing with Viilu's observation, but the point of transition moved progressively downstream with increasing  $R$  in the range  $R \lesssim 300$ . Around  $R = 300$  Reynolds found very long laminar jets corroborating Schade's observation. With further increase in  $R$ , of course, the transition point moved closer to the jet exit. The present visualization results, in the  $R$ -range covered, agree with the trend described by Reynolds. Such a trend, in regards to the stability and transition of a laminar jet, has remained unexplained on analytical grounds.

On the transition location, there is some difference between the measurements in the air jet (Table 3) and the visualization pictures (Fig. 6). Referring back to section 3.3, it would seem that the distance  $x_T$  should correspond to the laminar length terminated by the chaotic diffusion of the dye streaks in the visualization experiments. Accordingly, the laminar length at  $R \approx 1020$  can be estimated to be about  $25D$  from Fig. 6. This agrees with the data of Ref. 3, also based on visualization experiment. However, the  $x_T$  values listed in Table 3 are found to be larger, for example,  $70D$  at  $R \approx 1000$ . There could be various reasons for this discrepancy. First, the water jet environment was noisier in comparison to the anechoic housing of the air jet. Thus, there exists the possibility that ambient disturbances triggered faster transition in the water jet. A second, perhaps likelier possibility is the following.  $x_T$  was measured from hot-wire spectra in the air jets;  $x_T$

denoted the distance where the spectra were marked by a sudden increase in the broadband energy (Fig. 4). This location may not coincide with the location where the dye streaks get diffused. The instability is broadband and not periodic, and there is a significant shift in the frequencies within the distance  $x_I$  to  $x_T$ . Thus, the dye streaks could conceivably get diffused long before the evolution of broadband turbulence. Therefore, an impression of earlier than actual transition could be conveyed by the dye streaks.

In contrast, the values of  $x_I$  estimated from the visualization pictures agree reasonably with the hot-wire measurements in the air jet. This can be verified by inspection of Fig. 6 and comparison with corresponding data in Table 3.

In any case, the point pertinent to the present discussion is the nature of the instability wave leading to the transition. In all the pictures for  $R > 360$ , a helical instability (apparently with  $n = 1$ ), is quite clear prior to the transition. This confirms that the instability waves in the jets under consideration are primarily helical in nature, as predicted by the stability analyses.

### 3.5 Variation of the Strouhal Number

It is observed in Fig. 4 that the mean frequency of the spectral hump,  $f_m$ , gradually decreases with increasing  $x$ . The variation of the corresponding  $St$  with  $x/D$ , for different  $R$ , are shown in Fig. 7. Average straight lines, each having a slope of  $-0.003$ , seem to represent the data sets quite well. Note that the flagged data points were taken with probe 2 in a later repeat of the experiment. The data trends are found to be repeatable and consistent.

For a given  $x/D$ , a general dependence of  $St$  on  $R$  should also be evident from Fig. 7. Velocity spectra measured at  $x/D = 15$  for varying  $R$  are shown in Fig. 8. The corresponding variation of  $St$  with  $R$ , measured at different  $x/D$ , are presented in Fig. 9. A decreasing value of  $St$  with decreasing  $R$  is

clear. Note that below a Reynolds number of about 400, the velocities were too small to make reliable hot-wire measurements especially at large distances from the jet exit. However, clear spectral peaks, as in Figs. 4 and 8, were not detectable anywhere for  $R < 400$ . Actually, the repeatability of the data in the range  $R < 700$  was found to be poor in the original experiment; the data points in that range have been added after careful re-examination in the later experiment with probe 2.

Referring back to Fig. 7, one might expect that the decrease in  $St$  with  $x/D$  be accounted for by the corresponding changes in the local velocity and length scales. However, it was observed (Fig. 2(b)) that a typical length scale, e.g.,  $D_{0.5}$ , does not change appreciably. Thus, the variation of  $f_m$  may be expected to scale primarily with the local peak velocity  $U_c$ . A nondimensional frequency,  $2f_m D/U_c$ , measured for  $R = 1800$ , was indeed found to remain approximately constant at about 0.4, at all  $x$ . This value also equals the intercept of the straight line,  $St = St^* - 0.003x/D$ , through the corresponding data in Fig. 7. In a simplistic sense, the intercept  $St^*$  can thus be considered as a Strouhal number which would have remained the same everywhere had the velocity  $U_c$  (and the diameter) remained unchanged from the exit values.  $St^*$  is thus assumed to represent the preferred Strouhal number of the jets having the exit conditions, and is cross-plotted in Fig. 10 from the same data of Fig. 9. The Strouhal number clearly decreases with Reynolds number in the lower end of the  $R$ -range covered. A similar trend is also predicted by stability analysis, as elaborated in the following.

#### 4. COMPARISON WITH STABILITY ANALYSIS

An original stability analysis of axisymmetric flows is that of Batchelor and Gill.<sup>20</sup> Subsequently, flows with specific profiles were analyzed in detail including the viscous effects by, among others, Kambe,<sup>21</sup> Lessen and Singh,<sup>2</sup> and

Morris.<sup>23</sup> Predictions from these three analytical works are compared with the present results.

Kambe analyzed the jet with a parabolic profile, while Lessen and Singh as well as Morris analyzed the bell-shaped profile (see Fig. 11). Lessen and Singh carried out both temporal and spatial stability analysis, and the nondimensional frequencies corresponding to the maximum growth rates could be inferred from their Figs. 3 to 5. For the spatial case, the frequency corresponding to maximum growth rate ( $\alpha_i$ -maximum) at a given  $R$  was read directly from their Fig. 5. For the temporal case, loci of constant  $R$  curves had to be cross-plotted on the  $\alpha_i$  versus  $\alpha_r$  plane; from these, frequencies corresponding to the maximum temporal growth rate ( $\alpha_i$ -maximum) were obtained.

The  $\alpha_i$ -maxima could not be obtained from Kambe's<sup>21</sup> results, as his main objective was to determine the critical Reynolds number, and thus his analysis was confined to only a few low  $R$  cases. However, the present initial profile being parabolic (Fig. 2(a)) it was considered worthwhile to obtain the corresponding predictions following Kambe's analysis. Kambe's eigenvalue Eq. (6.11) was solved numerically, a brief description of which is given in the Appendix.

The predicted variations of Strouhal number with  $R$  are compared in Fig. 10 with the experimental data. It is clear that all three analyses predict a sharp increase in the Strouhal number with increasing  $R$  in the range  $R < 200$ . It is remarkable that despite involving temporal and spatial stability analyses of parabolic and bell-shaped profiles, all three predict very similar trends in this  $R$ -range. The temporal analysis of Kambe predicts an overshoot of the Strouhal number before asymptotically reaching the inviscid limit value--a trend not borne out by the experiment. It is not clear whether the temporal analysis of the bell-shaped profile would also predict a similar overshoot.

With the addition of two more data points at higher  $R$  provided by Ref. 23, it is apparent that the spatial stability analysis does not predict the overshoot and represents the experimental data trend better.

The inviscid limit predictions, shown at  $R = 4000$  in Fig. 10, are in general agreement with one another. The asymptotic experimental value is found to be somewhat higher. In passing, we note that Michalke's<sup>25</sup> inviscid analysis for the preferred mode of a top-hat jet, for the corresponding  $U$ -profile at  $x/D = 2$ , predicted a  $St$  of 0.35. Crighton and Gaster's<sup>26</sup> inviscid, linear stability analysis for a slowly diverging jet also predicted a preferred mode at  $St = 0.4$ .

Even though the spatial stability theory does reasonably well in the prediction there are obvious differences with the data. As noted before the inviscid limit value is underpredicted, by about 20 percent. A more serious discrepancy occurs on the low end of the  $R$ -range. The sharp decrease in  $St$  is predicted around  $R = 200$ ; (the curves should terminate on the left at the respective critical Reynolds numbers). The corresponding decrease in the data commences at a much higher  $R$  ( $\sim 600$ ). A source of the latter discrepancy may lie in the fact that the velocity profiles in these jets are still evolving and have not attained self-similarity (see discussion of Fig. 2(b)). Whereas parallel flow as well as an invariant shape of the mean velocity profile are assumed in all the analyses. It is, however, not clear if this would explain the discrepancy, and the analytical aspects leading to the difference were considered beyond the scope of the present study.

## 5. CONCLUDING REMARKS

The stability of low Reynolds number jets, issuing from fully developed tube flow, have been investigated by flow visualization and surveys of  $u'$ -spectra and the results compared with analytical predictions. The visualization confirmed that the instability is in a helical mode as predicted



by the analyses. The nondimensional frequency of the natural disturbance receiving maximum amplification, or the preferred Strouhal number, is found to depend on the Reynolds number. Experimentally, ensuring parabolic initial U-profile, the Strouhal number is found to increase with increasing  $R$ . It is clearly shown that a similar trend is also predicted (for the  $n = 1$  mode) by stability analysis of jets with representative U-profiles. Spatial stability analysis for the bell-shaped profile is found to yield predictions most closely agreeing with the experimental data. Differences remain in the predicted and the experimental results. The sharp drop in  $St$  with decreasing  $R$  is predicted around  $R = 200$ , the corresponding drop in the experiment commences at a higher  $R$  ( $\sim 600$ ).

## 6. ACKNOWLEDGEMENT

The first author held a NRC-NASA associateship during 1982-84 when the experiment was done originally, and with ESCON during 1984-85 when part of the analysis was done, at NASA Langley Research Center. Support from colleagues at NASA Lewis Research Center towards completion of the study is gratefully acknowledged. The authors would like to thank Mr. M.K. Ponton, Mr. J.C. Manning and Dr. J.C. Yu for help in various forms, and to Professors T. Kambe and C.K.W. Tam for helpful comments.

## APPENDIX

Diametral cross sections of the axisymmetric U-profiles analyzed by Kambe<sup>21</sup> and Lessen and Singh<sup>22</sup> are shown in Fig. 11. The reader may refer to either paper for the formulation of the governing equations for small disturbances of the form,  $\exp[i\alpha(x - ct) + in\phi]$ . In temporal analysis, the axial wavenumber  $\alpha$  is real and nonnegative,  $c = c_r + ic_i$  is the complex disturbance velocity,  $\alpha c_i$  being the exponential growth rate of the disturbance. The azimuthal wavenumber  $n$  is an integer (mode number); analysis for the first helical mode ( $n = 1$ ), which is the most unstable one, is only considered here. It can be shown that  $St = 3\alpha c_r/\pi$ , with  $r_0 = D/2$ , in Lessen and Singh's analysis, and  $St = 2\alpha c_r/\pi$  in Kambe's analysis, with  $St$  and  $D$  being in the present notations; ( $U$  and  $r$  are normalized and  $r_0$  the normalizing length scale in Fig. 11).

### Kambe's Solution

For finite  $\alpha R$ , for nonaxisymmetric disturbances ( $n \neq 0$ ), by matching the inner and outer solutions at  $r = 1$  (i.e., at the point of discontinuity, Fig. 11(a)), Kambe obtained the following eigenvalue equation.

$$\begin{vmatrix} K_{n-1}(\alpha) & K_{n-1}(\beta) & 0 & S_1 & S_2 & S_3 \\ \alpha K'_{n-1}(\alpha) & \beta K'_{n-1}(\beta) & 0 & S'_1 & S'_2 & S'_3 \\ \alpha^2 K''_{n-1}(\alpha) & \beta^2 K''_{n-1}(\beta) & 0 & S''_1 & S''_2 & S''_3 \\ K_{n+1}(\alpha) & 0 & K_{n+1}(\beta) & T_1 & T_2 & T_3 \\ \alpha K'_{n+1}(\alpha) & 0 & \beta K'_{n+1}(\beta) & T'_1 & T'_2 & T'_3 \\ \alpha^2 K''_{n+1}(\alpha) & 0 & \beta^2 K''_{n+1}(\beta) & T''_1 & T''_2 & T''_3 \end{vmatrix} = 0$$

where  $K_n$  is modified Bessel function of order  $n$ ,

$$\beta^2 = \alpha^2 - i\alpha R c$$

$$S = r^\mu \sum_{k=0}^{\infty} a_k r^{2k}, \quad T = r^\mu \sum_{k=0}^{\infty} b_k r^{2k},$$

$$\mu = n - 1, \quad k \geq 2,$$

$$a_{-1} = b_{-1} = b_0 = 0,$$

$$a_k = \frac{\gamma^2(k-1)a_{k-1} + i\alpha R\{b_{k-2} - (k-2)a_{k-2}\} + \frac{\alpha^2}{4n} f_k(a,b)}{4k(k-1)(m-1)}$$

$$b_k = \frac{\gamma^2(m-1)b_{k-1} + i\alpha R\{a_{k-2} - (m-2)b_{k-2}\} + \frac{\alpha^2}{4n} f_k(a,b)}{4m(m-1)(k-1)}$$

$$f_k(a,b) = 4(k-1)(m-2)a_{k-1} - 4(m-1)(k-2)b_{k-1}$$

$$- \gamma^2(a_{k-2} - b_{k-2}) + i\alpha R(a_{k-3} - b_{k-3}),$$

$$m = k + n, \quad \text{and} \quad \gamma^2 = \alpha^2 - i\alpha R(c-1).$$

Primes on  $S$  and  $T$  denote differentiation with respect to the radius,  $r$ ;  $S_j$  and  $T_j$  are obtained by equating the constants  $a_0, a_1, b_1$  to 1, 0, 0 cyclically.

For a given  $R$ , the eigenvalues  $c_i, c_r$  were obtained for varying  $\alpha$ . This provided the amplification rate  $\alpha c_i$  versus  $St$ , which is shown in Fig. 12, for a few  $R$ . The preferred Strouhal number denoted by  $\alpha c_i$ -maximum was thus calculated for up to  $R = 1200$ .

## REFERENCES

1. Viilu, A.: An Experimental Determination of the Minimum Reynolds Number for Instability in a Free Jet. *J. Appl. Mech.*, vol. 29, no. 3, Sept. 1962, pp. 506-508.
2. Reynolds, A.J.: Observations of a Liquid-Into-Liquid Jet. *J. Fluid Mech.*, vol. 14, pt. 4, Dec. 1962, pp. 552-556.
3. McNaughton, K.J.; and Sinclair, C.C.: Submerged Jets in Short Cylindrical Flow Vessels. *J. Fluid Mech.*, vol. 25, pt. 2, June 1966, pp. 367-375.
4. Andrade, E.N. Da C.: The Sensitive Flame. *Proc. Phys. Soc.*, vol. 53, pt. 4, no. 298, July 1, 1941, pp. 329-355.
5. Crow, S.C.; and Champagne, F.H.: Orderly Structure in Jet Turbulence. *J. Fluid Mech.*, vol. 48, pt. 3, Aug. 16, 1971, pp. 547-591.
6. Perry, A.E.; and Lim, T.T.: Coherent Structures in Coflowing Jets and Wakes. *J. Fluid Mech.*, vol. 88, pt. 3, Oct. 13, 1978, pp. 451-463.
7. Michalke, A.; and Wille, R.: Stromungsvorgange in Laminar-Turbulenten Übergangsbereich von Freistrahlgrenzschichten (Flow Phenomena in the Laminar-Turbulent Transition Zone of Free-Jet Boundary Layers). *Proceedings of the 11th International Congress for Applied Mechanics*, H. Gortler, ed., Springer-Verlag, Berlin, 1964, pp. 962-972.
8. Beavers, G.S.; and Wilson, T.A.: Vortex Growth in Jets. *J. Fluid Mech.*, vol. 44, pt. 1, Oct. 21, 1970, pp. 97-112.
9. Anderson, A.B.C.: A Jet-Tone Orifice Number for Orifices of Small Thickness-Diameter Ratio. *J. Acoust. Soc. Am.*, vol. 26, no. 1, Jan. 1954, pp. 21-25.
10. Anderson, A B C.: Metastable Jet-Tone States of Jets from Sharp-Edged Circular, Pipe-Like Orifice. *J. Acoust. Soc. Am.*, vol. 27, no. 1, Jan. 1955, pp. 13-21.

11. Unfried, H.H.: An Approach to Broadband Fluid Amplification at Acoustic Frequencies. Proceedings of the Fluid Amplification Symposium, Vol. 1, Harry Diamond Labs, Washington, DC, 1965, pp. 267-296 (Avail. NTIS, AD-623455.)
12. Browand, F.K.; and Laufer, J.: The Role of Large-Scale Structures in the Initial Development of Circular Jets. Turbulence in Liquids, J.L. Zakin, and G.K. Patterson, eds., Science Press, Princeton, NJ, 1975, pp. 333-344.
13. Rockwell, D.O.: The Macroscopic Nature of Jet Flows Subjected to Small Amplitude Periodic Disturbances. Sonochemical Engineering, AIChE Chem. Eng. Prog. Symp. Ser., vol. 67, no. 109, 1971, pp. 99-107.
14. Wyganski, I.; and Fiedler, H.: Some Measurements in the Self-Preserving Jet. J. Fluid Mech., vol. 38, pt. 3, Sept. 18, 1969, pp. 577-612.
15. Bradshaw, P.: An Introduction to Turbulence and its Measurement. Pergamon Press, New York, 1971.
16. Ligrani, P.M.; and Bradshaw, P.: Spatial Resolution and Measurement of Turbulence in the Viscous Sublayer Using Subminiature Hot-Wire Probes. Exper. Fluids, vol. 5, no. 6, 1987, pp. 407-417.
17. Freymouth, P.: Engineering Estimate of Heat Conduction Loss in Constant Temperature Thermal Sensors. TSI Quarterly, vol. 5, no. 3, Aug.-Sept. 1979, pp. 3-8.
18. Kibens, V.: The Limits of Initial Shear-Layer Influence on Jet Development. AIAA Paper 81-1960, Oct. 1981.
19. Hussain, A.K.M.F.; and Zaman, K.B.M.Q.: An Experimental Study of Organized Motions in the Turbulent Plane Mixing Layer. J. Fluid Mech., vol. 159, Oct. 1985, pp. 85-104.
20. Batchelor, G.K.; and Gill, A.E.: Analysis of the Stability of Axisymmetric Jets. J. Fluid Mech., vol. 14, pt. 4, Dec. 1962, pp. 529-551.

21. Kambe, T.: The Stability of an Axisymmetric Jet with Parabolic Profile.  
J. Phys. Soc. Jpn., vol. 26, no. 2, Feb. 1969, pp. 566-575.
22. Lessen, M.; and Singh, P.J.: The Stability of Axisymmetric Free Shear  
Layers. J. Fluid Mech., vol. 60, pt. 3, Sept. 18, 1973, pp. 433-457.
23. Morris, P.J.: The Spatial Viscous Instability of Axisymmetric Jets.  
J. Fluid Mech., vol. 77, pt. 3, Oct. 8, 1976, pp. 511-529.
24. Schlichting, H.: Boundary Layer Theory. 7th edition, McGraw-Hill,  
New York, 1979.
25. Michalke, A.: Instability of a Compressible Circular Free Jet with  
Consideration of the Influence of the Jet Boundary Layer Thickness. NASA  
TM-75190, 1971.
26. Crighton, D.G.; and Gaster, M.: Stability of Slowly Diverging Jet Flow.  
J. Fluid Mech., vol. 77, pt. 2, Sept. 24, 1976, pp. 397-413.

TABLE 1. - SCALING OF PREFERRED FREQUENCY ( $f_m$ ) IN LOW REYNOLDS  
NUMBER JETS FROM VARIOUS NOZZLES

[R is Reynolds number based on average exit velocity ( $U_{av}$ ),  
and  $St = f_m D / U_{av}$ .]

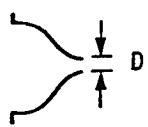
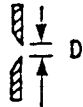
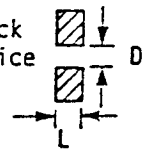
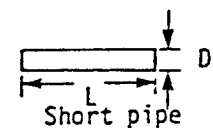
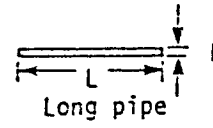
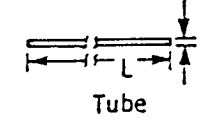
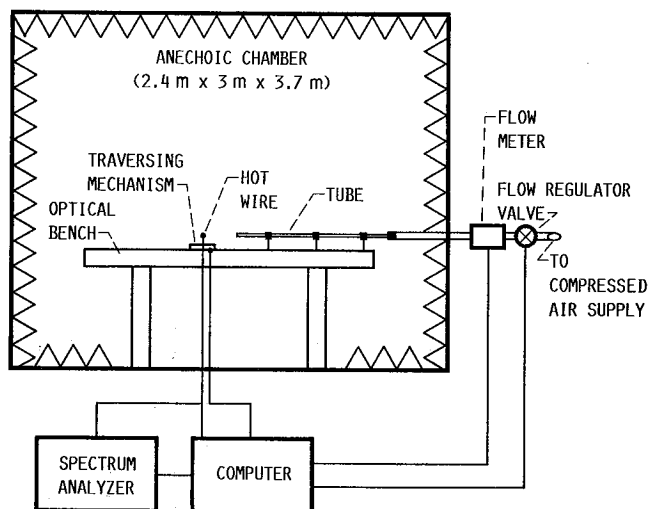
Nozzle geometry	Investigator (U-profile)	R	L/D	$f_m$ -scaling
	Michalke and Willie <sup>7</sup> (Top-hat thin boundary layer)	>5000	----	$St \propto R^{0.5}$
Sharp orifice 	Beavers and Wilson <sup>8</sup>	600-2800	0	$St \approx 0.63$
Thick orifice 	Anderson <sup>9</sup>	>3000 ~	0.5-1.25	$f_m L / U_{av} \approx 0.7$
 Short pipe	Anderson <sup>10</sup>	1100-2100	$\left\{ \begin{array}{l} < 8 \\ \sim \\ > 8 \end{array} \right.$	$f_m L / U_{av} \approx n/2 + 0.1$ in each integral stage, n
 Long pipe	Unfried <sup>11</sup> (Parabolic?)	800-3000		$St \approx 0.4$
 Tube	Present (Top-hat thick boundary layer)	$10^4 - 3 \times 10^4$	168	$St \approx 0.4$
	Present (Parabolic)	400-4000	600	?

TABLE 2. - CHARACTERISTICS OF THE HOT-WIRE PROBES  
[Dimensions are in millimeters.]

Probe number	Diameter	Active length	Aspect ratio	Prong-to-prong distance	Make
1	5	1.25	250	3	DISA 55P01
2	2.5	.64	256	.8	-----
3	5	1.25	250	1.25	DISA 55P11
4	5	6.35	1270	6.35	-----

TABLE 3. - POINTS OF INSTABILITY ( $x_I$ ) AND  
TRANSITION ( $x_T$ ) AT DIFFERENT R

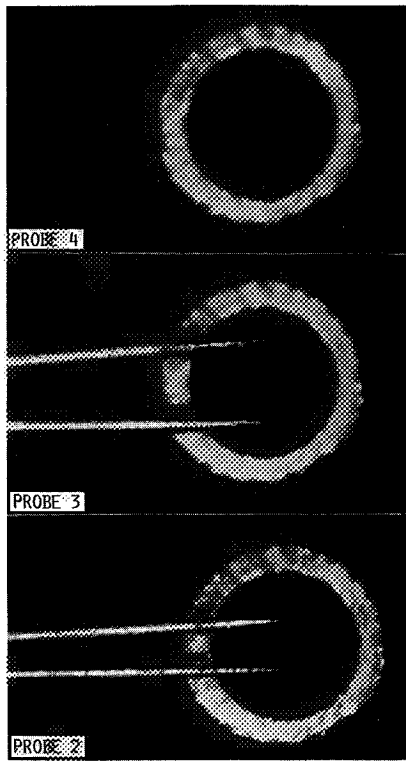
R	660	950	1480	2000	2800
$x_I/D$	15	15	12.5	11.5	10
$x_T/D$	>70	70	36	30	25



1(a) SCHEMATIC OF EXPERIMENTAL SETUP AND INSTRUMENTATION.

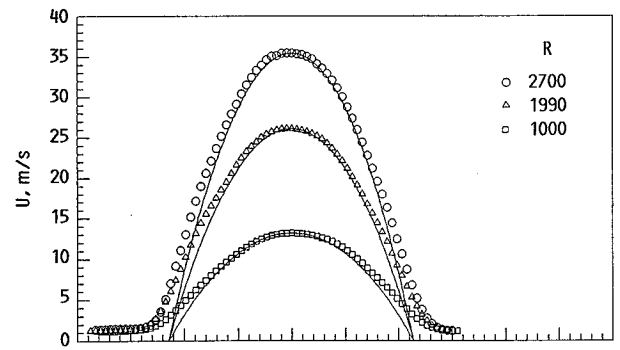
FIGURE 1. - EXPERIMENTAL FACILITY.



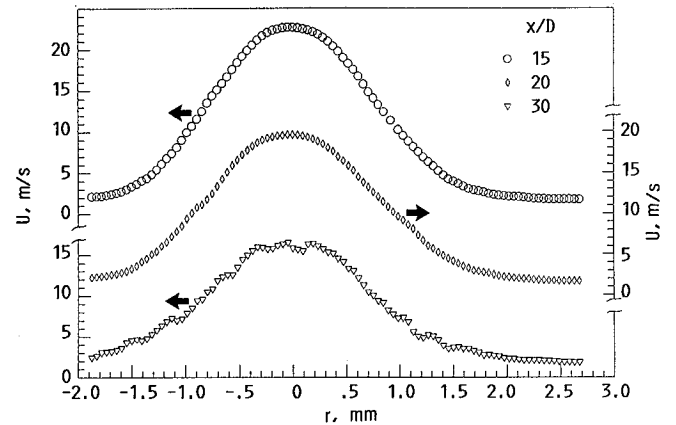


1(b) PICTURES OF HOT-WIRE PROBES 2 TO 4 (SEE TABLE 2) WITH 2.3 mm TUBE EXIT AS BACKGROUND.

FIGURE 1. - CONCLUDED.



(a) U-PROFILES MEASURED BY PROBE 2 AT JET EXIT,  $x/D \approx 0.5$ .



(b) U-PROFILES AT DIFFERENT  $x/D$  FOR  $R = 2000$ ; PROBE 2.

FIGURE 2. - MEAN VELOCITY ( $U$ ) PROFILES.

ORIGINAL PAGE  
BLACK AND WHITE PHOTOGRAPH

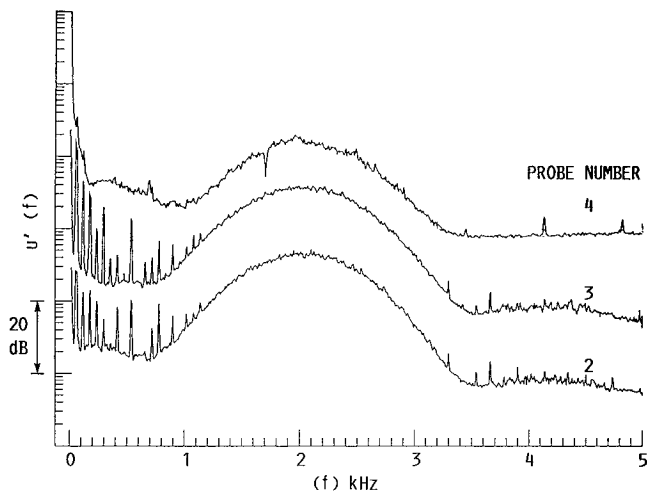


FIGURE 3. -  $u'$ -SPECTRA MEASURED AT  $x/D = 20$  ON THE JET AXIS, FOR  $R = 2000$ , WITH DIFFERENT PROBES. (ARBITRARY VERTICAL SCALES.)

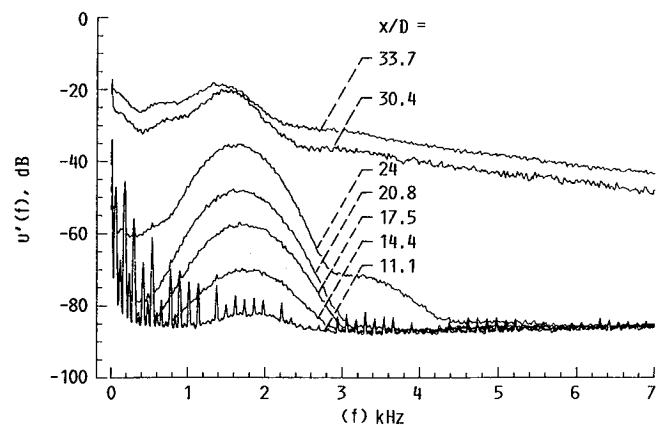


FIGURE 4. -  $u'$ -SPECTRA MEASURED ON THE AXIS OF THE JET AT DIFFERENT  $x/D$ ;  $R = 1800$ , PROBE 1. (ARBITRARY BUT SAME VERTICAL SCALES.)

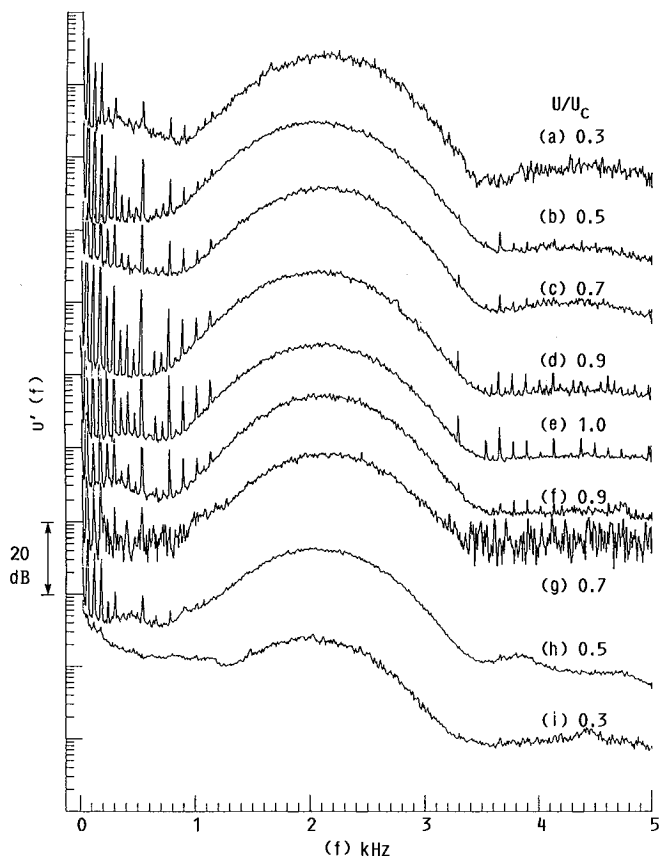


FIGURE 5. -  $u'$ -SPECTRA MEASURED AT DIFFERENT RADIAL LOCATIONS; LOCAL VELOCITY INDICATED FOR EACH CURVE.  $R = 2000$ ,  $x/D = 20$ , PROBE 2. CURVES ARE STAGGERED. (ARBITRARY BUT SAME VERTICAL SCALES.)

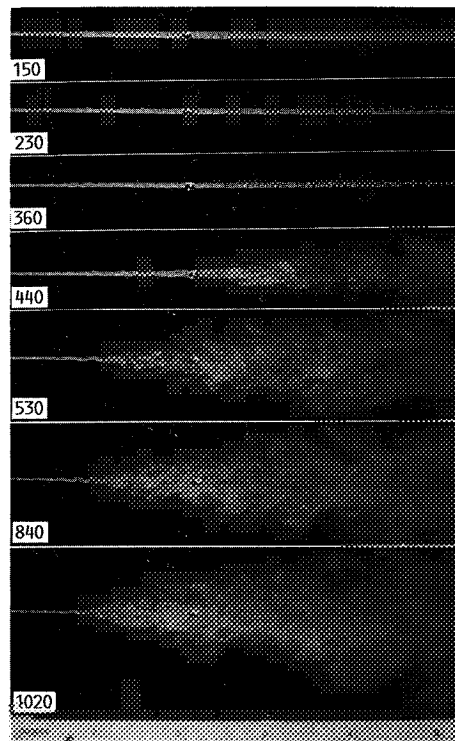


FIGURE 6. - FLOW VISUALIZATION PICTURES FOR WATER-IN-WATER JETS AT INDICATED REYNOLDS NUMBERS. JET WITH FLUORESCENT DYE ISSUED INTO STILL WATER;  $D = 1.1$  mm;  $L/D \cong 600$ .

ORIGINAL PAGE  
BLACK AND WHITE PHOTOGRAPH

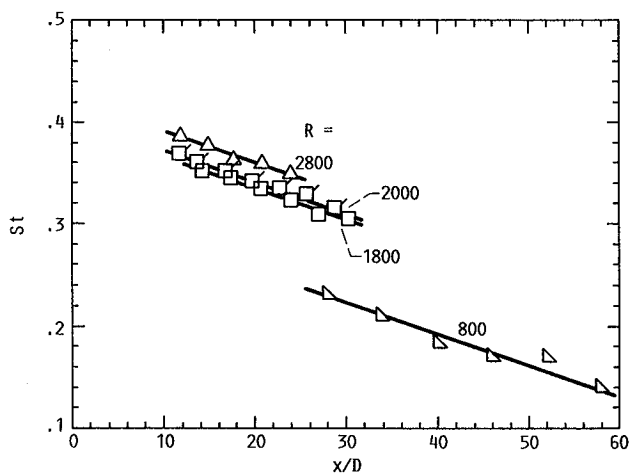


FIGURE 7. - VARIATION OF STROUHAL NUMBER  $St (= f_m D / U_{av})$ , CORRESPONDING TO SPECTRAL PEAKS AS IN FIG. 4, WITH  $x/D$ ; REYNOLDS NUMBERS INDICATED. FLAGGED DATA TAKEN WITH PROBE 2, REST WITH PROBE 1.

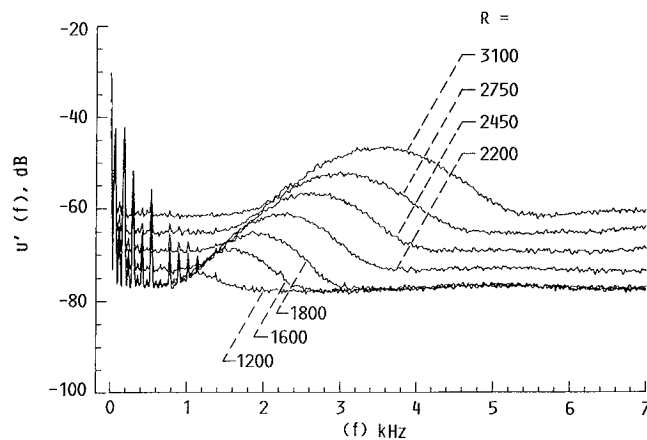


FIGURE 8. -  $u'$ -SPECTRA AT  $x/D = 15$  ON THE JET AXIS FOR DIFFERENT  $R$ , MEASURED WITH PROBE 1. (ARBITRARY BUT SAME VERTICAL SCALES.)

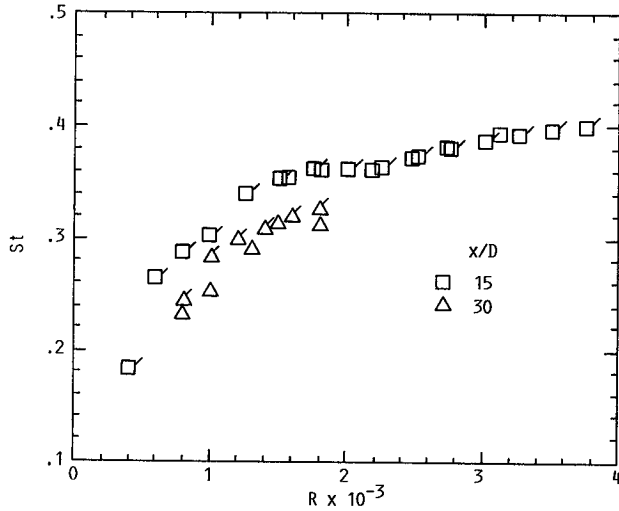


FIGURE 9. - VARIATION OF  $St$ , CORRESPONDING TO SPECTRAL PEAKS AS IN FIG. 8, WITH  $R$ . FLAGGED DATA TAKEN WITH PROBE 2, REST WITH PROBE 1.

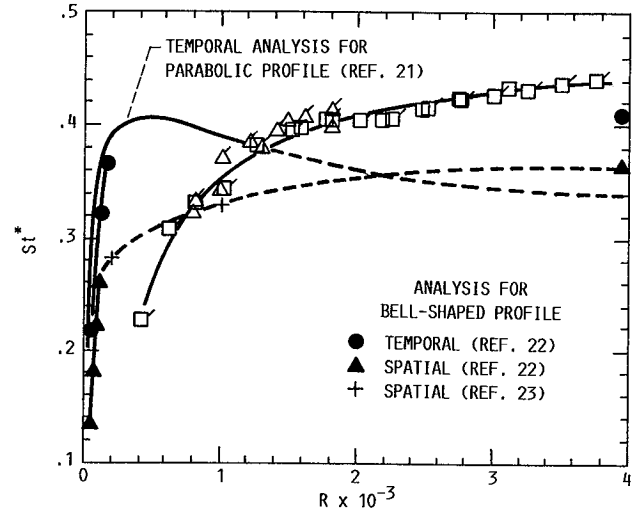
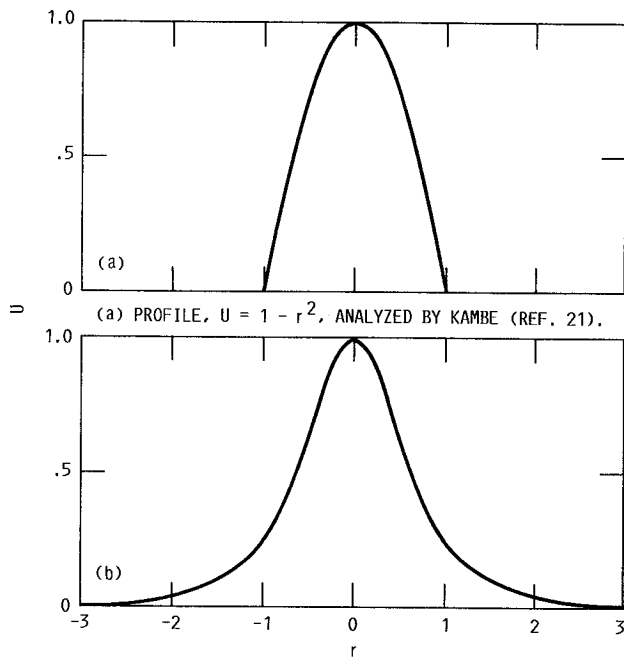


FIGURE 10. - VARIATION OF  $St^*$  ( $= St + 0.003x/D$ ) WITH  $R$ , FOR THE SAME DATA OF FIG. 9, COMPARED TO STABILITY ANALYSIS PREDICTIONS.



(b) PROFILE,  $U = 1/(1 + r^2)^2$ , ANALYZED BY LESSEN AND SINGH (REF. 22) AND MORRIS (REF. 23).

FIGURE 11. -  $U$ -PROFILES FOR STABILITY ANALYSIS.

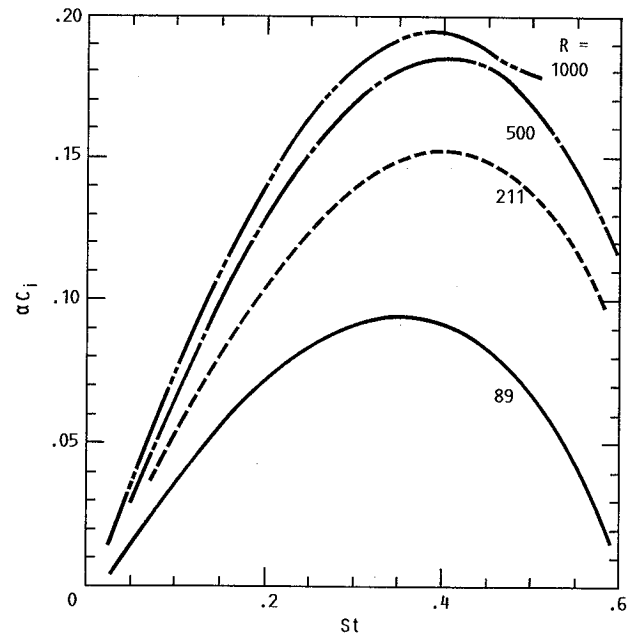


FIGURE 12. - (TEMPORAL) AMPLIFICATION RATE ( $\alpha_{c_i}$ ) VERSUS  $St$  ( $= 2\alpha_c/\pi$ ) FOR THE PROFILE OF FIG. 11(a); OBTAINED BY NUMERICALLY SOLVING KAMBE'S (REF. 21) EIGENVALUE EQ. (6.11).



## Report Documentation Page

1. Report No. NASA TM-102396		2. Government Accession No.		3. Recipient's Catalog No.	
4. Title and Subtitle Viscous Effects on the Instability of an Axisymmetric Jet				5. Report Date February 1990	
				6. Performing Organization Code	
7. Author(s) K.B.M.Q. Zaman and J.M. Seiner				8. Performing Organization Report No. E-4152-1	
				10. Work Unit No. 505-62-21	
9. Performing Organization Name and Address National Aeronautics and Space Administration Lewis Research Center Cleveland, Ohio 44135-3191				11. Contract or Grant No.	
				13. Type of Report and Period Covered Technical Memorandum	
12. Sponsoring Agency Name and Address National Aeronautics and Space Administration Washington, D.C. 20546-0001				14. Sponsoring Agency Code	
15. Supplementary Notes K.B.M.Q. Zaman, NASA Lewis Research Center; J.M. Seiner, NASA Langley Research Center, Hampton, Virginia 23665.					
16. Abstract  The stability characteristics of a laminar, axisymmetric jet, issuing from fully developed Poiseuille flow, are investigated. The jet preferred frequency, as inferred from surveys of $u'$ -spectra, is found to yield a Strouhal number ( $St$ ) that depends on the Reynolds number ( $R$ ); $St$ and $R$ are based on the jet diameter ( $D$ ) and the average velocity ( $U_{av}$ ) at the jet origin. The value of $St$ increases with increasing $R$ in the range $400 \leq R \leq 4000$ , attaining an asymptotic value of about 0.45. Flow visualization confirms that the instability is primarily in a helical mode, as predicted by stability analyses. Analyses do predict a similar $St$ versus $R$ variation in approximately the correct $St$ -range. However, the $R$ -range where this is predicted is lower than that found experimentally.					
17. Key Words (Suggested by Author(s)) Jets Instability Strouhal number Viscous effect				18. Distribution Statement Unclassified—Unlimited Subject Category 02	
19. Security Classif. (of this report) Unclassified		20. Security Classif. (of this page) Unclassified		21. No. of pages 28	
				22. Price* A03	